Electrochimica Acta 178 (2015) 813–822

Contents lists available at ScienceDirect

Electrochimica Acta

journal homepage: www.elsevier.com/locate/electacta

Key role of anions in the 2D–3D electrochemical deposition of Rh on Ag electrodes

Eduardo. N. Schulz[a,b,*], Andrés Ruderman[b,c], Germán J. Soldano[b,d], Silvana G. García[a], Elizabeth Santos[b,c]

[a] Instituto de Ingeniería Electroquímica y Corrosión, (INIEC)—Universidad Nacional del Sur, Bahía Blanca, Argentina
[b] Institute of Theoretical Chemistry, Ulm University, Ulm, Germany
[c] Instituto de Física Enrique Gaviola (IFEG-CONICET)—Universidad Nacional de Córdoba, Córdoba, Argentina
[d] INFIQC—Departamento de Matemática y Física Facultad de Ciencias Químicas—Universidad Nacional de Córdoba, Argentina

ARTICLE INFO

Article history:
Received 16 April 2015
Received in revised form 14 August 2015
Accepted 14 August 2015
Available online 20 August 2015

Keywords:
Rh
electrodeposition
growth mechanisms
ab initio thermodynamics
bimetallic systems

ABSTRACT

We have studied the electrochemical deposition of Rh on polycrystalline Ag substrates from electrolytes containing chloride and sulphate anions. Chronoamperometry and cyclic voltammetry have been employed in order to elucidate the growth mechanism. Anions play a key role in the growth mechanism and the resulting structures. In the presence of sulphate anions Rh deposition follows a 3D nucleation—growth mechanism, while a 2D nucleation—growth is obeyed in the case of electrolytes containing chloride anions. Ab initio thermodynamics studies support the hypothesis that chloride anions stabilize the Rh deposition favouring a 2D mechanism at low overpotentials in good agreements with the experimental data.

© 2015 Published by Elsevier Ltd.

1. Introduction

The classical catalysts for electrochemical reactions of practical interest usually consist of expensive noble metals such as Pt, Pd and Rh [1]. In recent years electrochemists have learned to prepare such catalysts in the form of nanoparticles supported on cheaper substrates; the corresponding electrodes have a high specific area and are much cheaper than bulk materials [2–4]. In addition, the nanoparticles sometimes have different catalytic properties than their macroscopic counterparts.

This emerging science of electrochemical nanotechnology also offers the possibility to construct bimetallic structures with new catalytic properties. Examples of such structures are surface alloys, clusters or monolayers of a metal on a foreign substrate [5–10]. In this work, we study a particularly interesting case of the formation of a bimetallic catalyst: the deposition of rhodium on silver.

There are three classical mechanisms through which the growth of thin films can be analysed: (1) Frank-van der Merwe or layer-by-layer growth; (2) Volmer-Weber growth or growth through formation of three-dimensional clusters; and (3) Stranski-Krastanov growth or layer-by-layer growth followed by cluster growth [11]. The surface energy of rhodium 2.83 Jm-2 is much higher than that of silver (1.30 Jm-2) [12]. Therefore one would expect that the deposition of Rh on Ag would follow the Volmer-Weber mechanism of three-dimensional growth, and that small clusters of Rh on Ag would be unstable. However, we shall demonstrate in this work both by experiments and by theory, that anions play a pivotal role in the stability of these clusters.

Before examining the electrochemical situation, let us take a brief look at the deposition of Rh on Ag in uhv. Under these conditions a Ag-Rh-Ag sandwich is formed on the surface [12]. At room temperature, the thermal diffusion of Ag is negligibly slow and the growing film would be rough, but it would have some layer-by-layer quality, especially for the first 2-3 monolayers [12]. Since the phase diagram [13] indicates that less than 0.5 at. % of Rh is soluble in Ag at room temperature, both metals are hardly miscible and alloy formation can be disregarded.

Chang et al. [14] have shown that by an activated exchange of Rh adatoms with Ag surface atoms the Rh/Ag(100) system evolves toward the energetically favoured Ag/Rh/Ag(bulk) structure. At intermediate coverages nucleation and growth of mixed Rh/Ag ad-islands occurs simultaneously. L.D. Roelofs et al. [15], based on Monte Carlo kinetics simulations, proposed that the dominant mechanism of hole formation in this system involves the growth of vacancy islands via an upward exchange diffusion move.

* Corresponding author at: Instituto de Ingeniería Electroquímica y Corrosión, (INIEC)—Universidad Nacional del Sur, Bahía Blanca, Argentina.
Fax: +54 291 4595182.
E-mail address: nschulz@uns.edu.ar (E. N. Schulz).

http://dx.doi.org/10.1016/j.electacta.2015.08.071
0013-4686/© 2015 Published by Elsevier Ltd.

Li et al. [16] have found that the growth of overlayers of Rh on Ag(100), while suffering from easy interdiffusion of Ag in and onto Rh, does produce pseudomorphic, albeit mixed, overlayers.

In the case of electrodeposition, the electrochemical environment plays a key role in the structure of the formed film, and therefore completely different behaviour can be expected than at the metal-vacuum interface. Diverse mechanisms can be tuned by the applied potential. In addition, the presence of anions can stabilize or inhibit the formation of certain structures.

Kibler et al. [17] have investigated the electrochemical deposition of Rh on Au(111) from $RhCl_3$ in sulphuric acid media by means of in-situ STM and cyclic voltammetry. We expect some similarities between these results and ours. Au and Ag have very similar lattice constants and both are coinage metals. On Au Rh starts to deposit irreversibly around 200 mV versus SCE [17]. First a rhodium bilayer grows, the electrochemical behaviour of which is similar to that of a well-ordered Rh(111) surface. On top of the second Rh monolayer small, three-dimensional clusters are formed. Also, a phase transition in adlayers of Rh-Cl complexes was observed, similar to the process of adlayers of Pd-Cl complexes.

More recently, Arbib et al. [18] have also investigated the electrodeposition of Rh on Au. They have shown that the deposition of Rh proceeds through a nucleation and growth mechanism, and that the overall electrocrystallisation phenomenon can be described in terms of the Stranski–Krastanov mechanism predicting the nucleation and growth of the 3D Rh clusters on the top of a preformed 2D Rh phase.

Pletcher and Urbina have studied the effect of sulphate [19] and chloride [20] anions on the electrodeposition of Rh on vitreous carbon and copper. In both media Rh deposition occurs with a substantial overpotential.

The electrodeposition of Rh on vitreous carbon depends strongly on the preparation of the surface [20]. In a previous work, some of us [21] have demonstrated that on an activated glassy carbon (GC) substrate, the formation of Rh deposits involves a 2D–3D nucleation transition. An initial 2D progressive nucleation is observed at short times, which evolves into a 2D instantaneous nucleation process at more cathodic potentials. In both cases these 2D nucleation processes are followed by a 3D nucleation with diffusion controlled growth at longer times.

The goal of this work is to investigate the effect of anions such as chloride and sulphate on the stabilization of given Rh-Ag nanostructures. Which growth mechanism takes place according to the type of anions present in the electrochemical environment? What are the driving forces that determine if homogeneous monolayers or three-dimensional conglomerates are formed? The answer to these questions is of fundamental importance for the design of new electrocatalysts or for the electroplating research field. Our strategy to elucidate these issues is a combination of experimental and theoretical approaches.

2. Experimental

A silver polycrystalline wire with an exposed area of 0.314 cm^2 was employed as working electrode. Previous to the experiments, this electrode was chemically treated with KCN and H_2O_2, and following a flame annealing procedure [22]. Rh deposits were removed by potential sweep in a 0.1 M CrO_3 solution, prior to a brief dipping in concentrated nitric acid and a careful wash with milli-Q water.

In order to study the effect of anions on the deposition of Rh, the following solutions were employed: 5 mM Na_3RhCl_6 + 0.5 M NaCl (pH = 3.3) and 2.5 mM $Rh_2(SO4)_3$ + 0.05 M Na_2SO_4. All chemicals were of ultra-pure quality and the solutions were prepared with milli-Q water, which were purged with N_2 prior to each experiment.

All measurements were carried out at room temperature (298 K) in a conventional electrochemical cell. The reference electrode was a saturated calomel electrode (SCE) inside a Luggin capillary.

Measurements were carried out by a computer controlled Autolab, model AUT 84233, using NOVA 1.6 software.

Each electrochemical measurement was performed several times and proved to be well reproducible.

3. Results and discussion

3.1. Electrochemical response in sulphate-containing electrolytes

Fig. 1 shows the cyclic voltammetry response of a polycrystalline Ag electrode immersed in 2.5 mM $Rh_2(SO_4)_3$ + 0.05 M Na_2SO_4 solution at a potential scan rate of 20 mVs^{-1}. The voltammogram shows three peaks in the negative scan at −0.155 V (*I*), −0.330 V (*II*) and −0.500 V (*III*) and two peaks in the positive scan, at −0.185 V (*II'*) and −0.375 V (*III'*).

If the negative limit of the potential scan is shifted in the region where peak I is located, a well-defined nucleation loop appears [23]. A similar behavior has been found by Pletcher and Urbina [19] for the deposition of Rh on GC, although the position of this peak was at lower potentials (E_p = −0.440 V). Arbib et al. [18] have obtained this characteristic loop for Rh deposition on Au(100), as well as on a polycrystalline Au electrode. Therefore, Peak *I* can be assigned to a 3D nucleation and growth process for the new Rh deposits, as it will be confirmed later on by the chronoamperometric experiments. The theoretical electrodeposition potential of Rh/Rh^{3+} calculated from Nernst equation [24] for our experimental conditions, is much higher (0.52 V vs SCE) indicating that this process occurs with a large overpotential on Ag substrates. However, this overpotential is lower than that observed in the case of Rh electrodeposited on GC as substrate [19]. Rh deposits cannot be removed by making the potential more positive, mainly due to the formation of an oxide film that passivates the deposits [25].

Another interesting feature is that peak *II'* is not observed when the scan limit is set to a potential value below peak *II*. This seems to indicate that these two peaks are related. Both peaks also show a linear dependence of the peak current on the scan rate indicating processes that take place under charge transfer control (not shown here, see Fig. S.1 in the Supporting Information (SI)). Therefore peak *II* must be related to the underpotential adsorption of hydrogen (H_{UPD}) on the newly formed Rh phase and peak *II'* can be due to the desorption of the H_{UPD}. Pletcher and Urbina [19,20] have

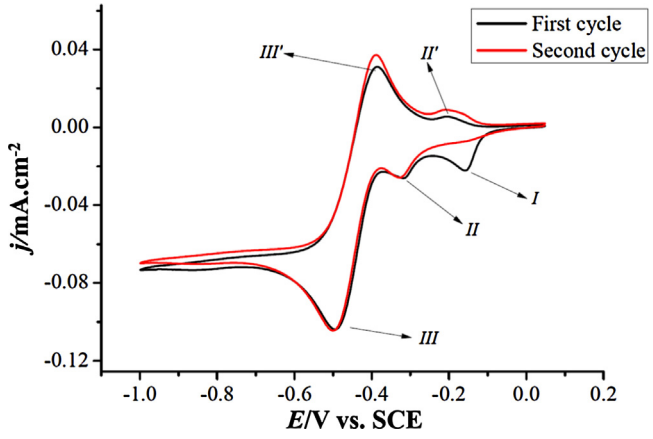

Fig. 1. Cyclic voltammogram of a polycrystalline silver electrode obtained in 2.5 mM of $Rh_2(SO_4)_3$ + 0.05 M Na_2SO_4. Scan rate: 20 $mV\,s^{-1}$.

also observed these processes on Rh deposited on GC. Although an irreversibility is already observed for the adsorption/desorption of hydrogen on Rh monocrystalline electrodes [26], in our case is much more pronounced. There are several possible reasons for this effect. It could be due to the partially irreversible oxidation of Rh at higher pH. Such an irreversibility is usually also related to a competition of adsorbed hydrogen with adsorbed anions [27]. Furthermore, the 3D growth of Rh can produce nanostructures showing high index orientation [28], which causes complex adsorption processes.

Concerning peaks *III* and *III'*, both show a linear dependence of the peak current on the square root of the scan rate (not shown here, see Fig. S.2 in the SI). This behavior is characteristic of a process under mass transfer control. Experimentally, the formation of small gas bubbles was observed at the beginning of peak *III*, suggesting that this peak is due to the reversible hydrogen evolution reaction. Therefore peaks *III/III'* can be assigned to the global reaction: $2H^+ + 2e^- \rightleftharpoons H_2$. This observation is in agreement with similar results for Rh deposits on glassy carbon substrates [19–21].

In order to obtain more information, we have performed chronoamperometric experiments by the application of potential steps from 0 V to the potential region around peaks *I*,*II* and *III*.

The chronoamperometric response obtained by application of potential steps in the potential range around peak *I* (from −0.190 V to -0.100 V) can be observed in Fig. 2. These current-transient curves show the characteristic shape of a charge-controlled process, similar to the deposition of PbO_2 on GC through a mechanism involving progressive nucleation 3D-growth [29]. This observation is in good agreement with the linear dependence of the peak *I* current on the potential scan rate.

Fig. 3 shows the chronoamperometric response around peak II obtained by potential pulses from 0 V to values between −0.350 V and −0.270 V. At potentials below peak II the process starts like a 3D deposition, as it is evident from the classical bell shape of the transient with a long tail. At potentials higher than the peak *II*, the response evolves into a more complex shape, and a second deposition process apparently starts. Similar coupled deposition processes were obtained by Palomar-Pardavé [30] and Schulz et al. [21] for the deposition of Rh from 5 mM Na_3RhCl_6 + 0.5 M NaCl solutions onto an electrochemically activated glassy carbon electrode. After the transient maximum the current decays to a stationary state following the Cottrell law for diffusional controlled process, in agreement with the results obtained by cyclic voltammetry described above.

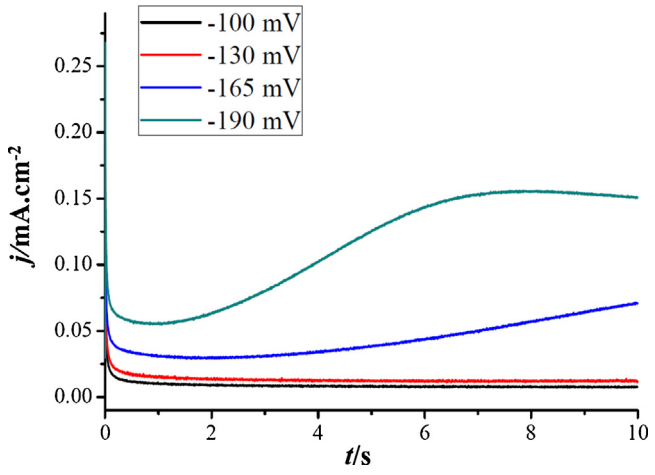

Fig. 2. Transients family recorded at potentials around the peak I in 2.5 mM of $Rh_2(SO_4)_3$ + 0.05 M Na_2SO_4. The potential was stepped from 0 V.

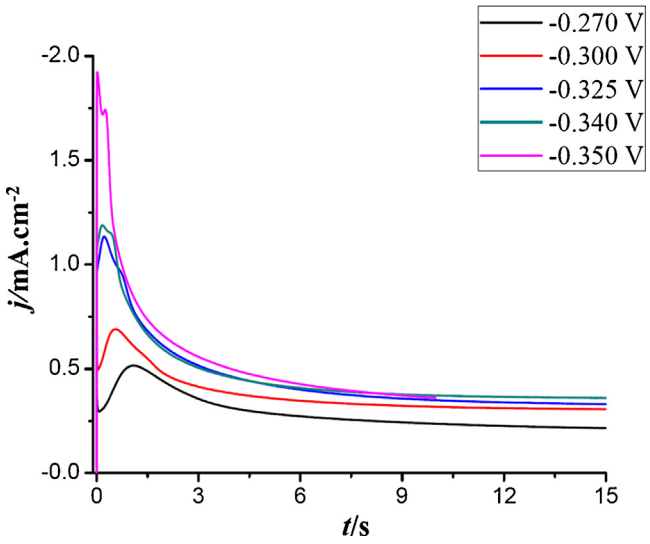

Fig. 3. Transients family recorded at potentials around the peak II in 2.5 mM of $Rh_2(SO_4)_3$ + 0.05 M Na_2SO_4. The potential was stepped from 0 V.

In the potential region of peak *III*, the response shows a continuous decay of the current with the typical hyperbolic-shape found in other works [19].

At higher overpotentials, mass transfer controls the process of Rh deposition. In this case, a current decay is obtained in the chronoamperometric response characteristic of Cotrell's regime of semi-infinite planar diffusion.

3.2. Electrochemical response in chloride-containing electrolytes

Fig. 4 shows the voltammetric response for the deposition of Rh from a 5 mM Na_3RhCl_6 + 0.5 M NaCl solution at a scan rate of 20 mVs^{-1}. Several peaks corresponding to different processes are observed, which will be analysed in detail. On the first negative scan, a peak appears at $E = -0.150$ V, which corresponds to two different processes. Effectively, this peak splits at higher potential scan rates, since the involved processes show a different dependence on scan rates. The first process appearing during the first negative scan can be attributed to rhodium deposition. The equilibrium potential calculated by using Nernst's equation is $E_{eq} = 0.19$ V for our conditions. Given the fact that this potential is more positive than the potential at which peak I starts, the underpotential deposition (UPD) of Rh is discarded as an explanation for this peak. During the second potential scan, Rh deposition starts at a more positive potential, closer to the calculated equilibrium potential for the couple Rh^{3+}/Rh. This is because the overpotential required to deposit Rh over previous Rh deposits is lower than that required for Rh deposition on Ag. The second process that becomes evident at higher scan rates can be assigned to the underpotential deposition of hydrogen on the freshly deposited Rh. Since rhodium deposition is a diffusion controlled process, it depends linearly on the square root of the scan rate, whilst the process due to hydrogen adsorption depends linearly on the scan rate (not shown here, see Fig. S.3 in the SI). This difference in the dependence with the scan rate allows us to separate the two peaks by simply varying the scan rate in the voltammetric experiments (see upper inset in Fig. 4).

In the potential region between −0.175 V and −0.200 V a nucleation loop can be observed, i.e. a range of potentials in which the cathodic current is higher than the anodic current (see inset at the bottom of Fig. 4). The crossover potential is $E_{co} = -0.200$ V, but it is not well defined due to the formation of a passivating oxide layer [21]. According to Fletcher et al. [23], under charge transfer

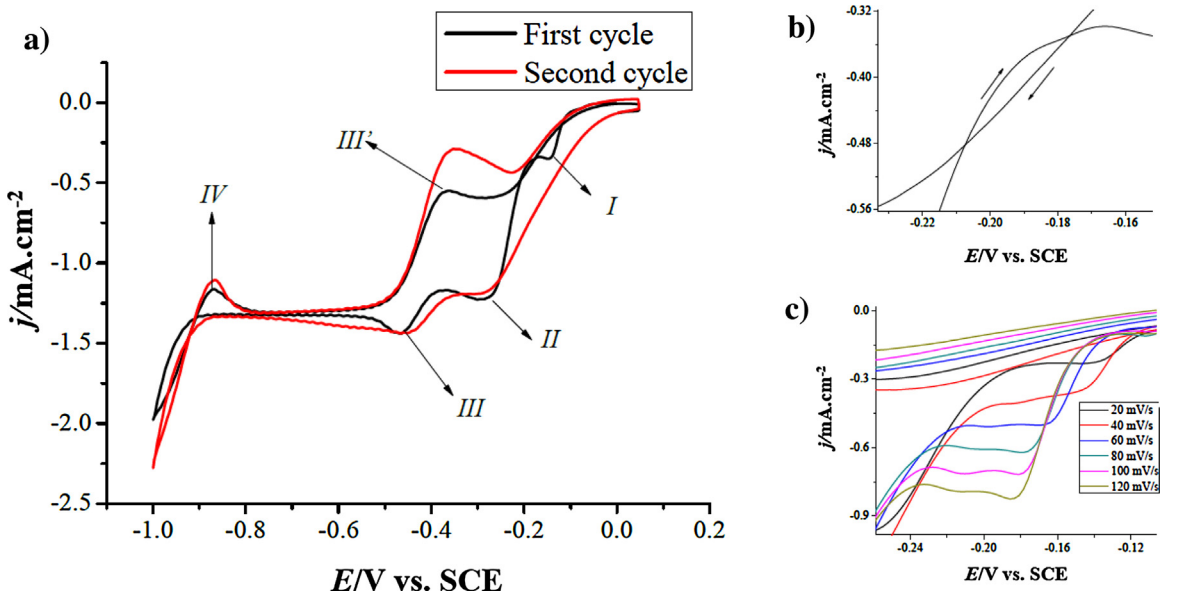

Fig. 4. (a) Cyclic voltammograms of a polycrystalline silver electrode obtained in 5 mM Na_3RhCl_6 + 0.5 M NaCl. Scan rate: 20 mV s^{-1}. (b) Zoom of the characteristic nucleation loop, (c) the split of peak I at higher scan rates (black line: 20 mV s^{-1}, red line: 40 mV s^{-1}, blue line: 60 mV s^{-1}, green line: 80 mV s^{-1}, pink line: 100 mV s^{-1}, dark yellow line: 120 mV s^{-1}).

control the E_{co} value should correspond to the equilibrium potential of the metal redox couple. However, in this case this potential cannot be directly related to the equilibrium potential of the redox couple due to the irreversibility of the Rh deposition process [23], and the presence of different complex ions of the form $[RhCl_n(H_2O)_{6-n}]^{3-n}$, $[RhCl_5(H_2O)]^{2-}$ and $[RhCl_4(H_2O)_2]^{-}$, the latter being the dominating species [20].

The peak denoted as *II* at $E = -0.300$ V shows the characteristic shape of a 3D nucleation mechanism followed by a rapid growth of the new phase under diffusional control [14]. This was also confirmed by chronoamperometric experiments. The trend followed by the current peak *II* is linear with the square root of the scan rate, which could be associated with rhodium deposition and growth under mass control. According to Pletcher et al. [20], after the rhodium deposition process takes place, the hydrogen evolution seems to occur in two distinct steps, the first being represented by peak *III* at −0.450 V, and the second step corresponding to the increase in current observed at E = −0.900 V. The voltammogram shown in Fig. 5 of a Rh(111) electrode in 0.5 M NaCl solution in the absence of Rh^{3+} ions supports the idea that these responses are not related to electrodeposition processes of the metal. Although the potentials are slightly shifted, one can clearly distinguish a small peak *I* at −0.212 V corresponding to the UPD of hydrogen, the first step for the hydrogen evolution (peak *III* at −0.400 V) and the starts of the massive evolution reaction around −0.900 V. The peak *II* corresponding to the 3D nucleation of Rh is obviously absent.

In order to analyze in more detail the Rh electrodeposition process, a family of current transients was recorded around peak *I* by selecting an initial potential of 0 V where no deposition of Rh is detected in the cyclic voltammogram (see Fig. 6). After the first decay due to double layer charging, the current increases to a maximum with an inverted parabola shape, characteristic of a 2D deposition process. In the case of the potential steps to −0.120 V and −0.130 V, the current subsequently drops off, tending to a constant value, which indicates that Cotrell's semi-infinite diffusion regime has been reached, also confirmed by the linear relation between the current and the inverse of the square root of time (see Fig. S.4 in SI). On the contrary, for the potentials steps to −150 mV and −170 mV, a 3D growth bell-shape can be seen after

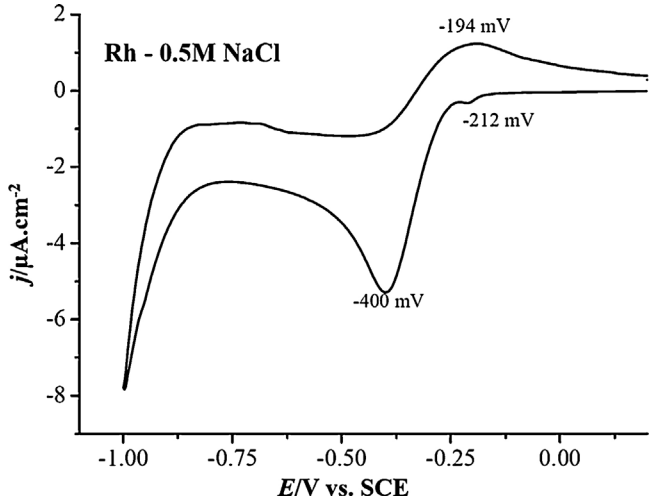

Fig. 5. Cyclic voltammogram obtained with a Rh(111)-electrode in a 0.5 M NaCl solution in the absence of Rh^{3+} ions. Scan rate: 20 mV/s.

the appearance of the 2D peak. This is a clear indication of a 2D-3D growth mechanism transition.

Fig. 7 shows a set of current transients recorded when the potential is stepped from 0 V to more negative values located in the region of potentials where peak *II* is observed. After the current drop due to the double layer charging a shoulder appears, which probably corresponds to the formation and growth of Rh nuclei. At longer times, the transients exhibit the typical shape for a nucleation process with three-dimensional (3D) growth of nuclei limited by diffusion of the electroactive species [22]. After the current passes the maximum when the individual diffusion zones of adjacent nuclei overlap, it decays converging to a limiting current, which corresponds to the linear diffusion of the electroactive ions to the planar electrode. In this region the current follows the usual $t^{-1/2}$ dependence according to the Cottrell equation (not shown here, see Fig. S.5 in the SI).

Dimensionless plots with normalized current density and time scale with the corresponding values for the maximum are

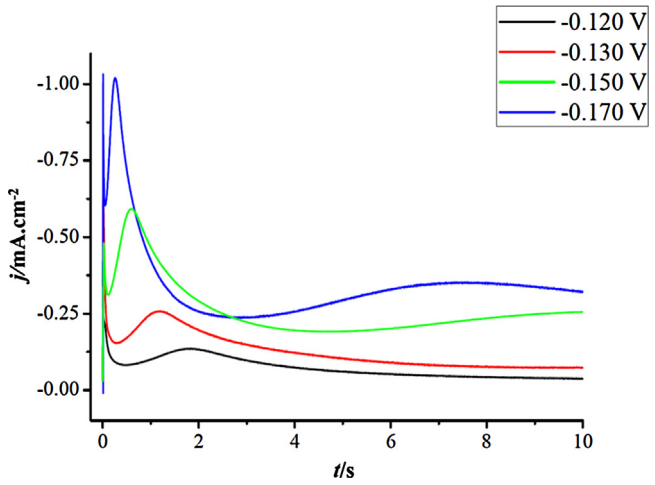

Fig. 6. Current transients for the nucleation of Rh on Ag recorded in the range of $-0.170 < E/V < -0.120$ in Na_3RhCl_6 5 mM + NaCl 0.5 M solution. The potential steps were applied from a starting potential of 0 V.

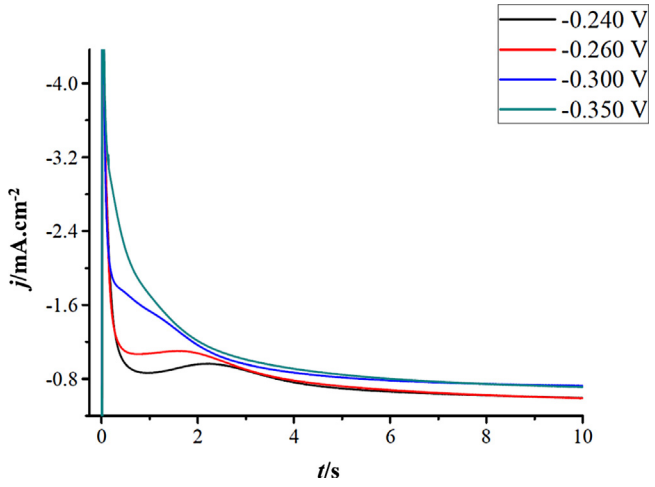

Fig. 7. Current transients set recorded in the range between −0.350 V and −0.240 V in Na_3RhCl_6 5 mM + NaCl 0.5 M solution. The potential steps were applied from 0 V.

particular suitable as a diagnostic criterion to determine the growth mechanism. Eqs. (1) and (2) [31] describe the behavior for an instantaneous and progressive growth in the 2D nucleation case:

$$\left(\frac{j}{j_{max}}\right)_{2D-Inst.} = \frac{t}{t_{max}} exp\left(-\frac{1}{2}\left(\frac{t^2 - t_{max}^2}{t_{max}^2}\right)\right) \quad (1)$$

$$\left(\frac{j}{j_{max}}\right)_{2D-Prog.} = \left(\frac{t}{t_{max}}\right)^2 exp\left(-\frac{2}{3}\left(\frac{t^3 - t_{max}^3}{t_{max}^3}\right)\right) \quad (2)$$

where j_{max} and t_{max} are the maximum current density and the time at which it is attained, respectively.

Similarly, Eqs. (3) and (4) proposed by Sharifker and Hills [32], describe the 3D growth mechanisms:

$$\left(\frac{j}{j_{max}}\right)^2_{3D-Inst.} = \frac{1.9542}{t/t_{max}}[1 - exp(-1.2564(t/t_{max}))]^2 \quad (3)$$

$$\left(\frac{j}{j_{max}}\right)^2_{3D-Prog.} = \frac{1.2254}{t/t_{max}}\left[1 - exp\left(-2.3367(t/t_{max})^2\right)\right]^2 \quad (4)$$

Fig. 8a and 8b shows the dimensionless plots for two different potentials in the regions of peak *I* and *II* respectively in comparison with the theoretical curves for the response according to the various mechanisms mentioned above.

These results clearly demonstrate that in the region of peak *I* the predominant process is an instantaneous nucleation and 2D growth of the deposit, while in the region of peak *II* a progressive nucleation and 3D growth occurs. In the latter case, at short time during the early parts of the rising transients, the overlap with other processes such as the double layer, makes the fit difficult. However, the fit is good at longer time intervals, where the effect of processes, such as the reorganization of the electrical double layer are negligible.

Some characteristic parameters can be obtained by fitting the experimental current transients. In the region where the 2D growth takes places (around peak *I*), the current response can be described through the following expression [17,31]:

$$j(t) = \frac{\pi z F M h N_0 k^2 t}{\rho} exp\left(\frac{\pi M^2 N_0 k^2 t^2}{\rho^2}\right) \quad (5)$$

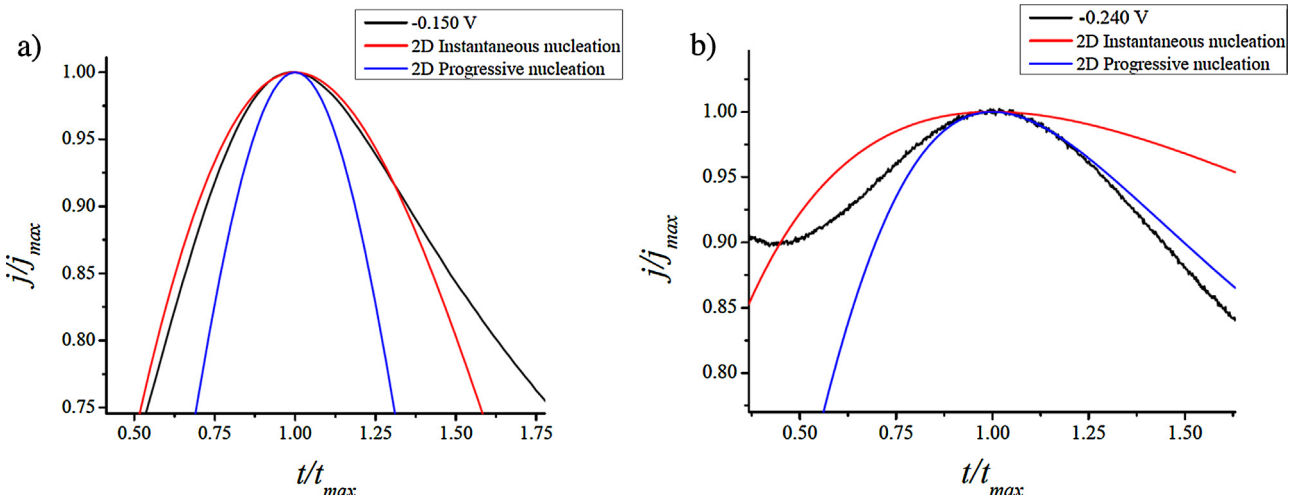

Fig. 8. Comparison between experimental and theoretical dimensionless curves for (a) the potential region of peak I and (b) the potential region of peak II. The black lines are experimental curves obtained for potential steps to −0.150 V and −0.240 V. The blue and red lines represent the theoretical curves calculated using Eqs. (1)–(4).

where F is the Faraday's constant, z the electron number involved in the reaction, M and ρ the rhodium atomic mass and density respectively, h the height of the monolayer, N_o the active site density number and k the 2D lateral growth rate constant.

Table 1 shows the results obtained using Eq. (5) to fit the experimental curves in the region of peak *I*. The values for the height h are reasonably good for up to two monolayers of Rh. These values also are in agreement with preliminary in situ STM studies of the Rh electrodeposition from solutions containing chloride ions [33], where small clusters of monoatomic height were found in this potential range during the first stage, which finally evolve to bilayers.

A logarithmic representation of $N_o k^2$ as a function of potential gives a linear dependence (see Fig. A.6 in the A). The slope indicates that the potential dependence is governed by the rate constant k, with a transfer coefficient of about 0.5 (see Fig. 9).

In the region of peak *II*, where the deposition of Rh takes place through a 3D growth mechanism, the current transients were analyzed using the approach proposed by Heerman and Tarallo [34]:

$$j(t) = zFDc\frac{1}{\sqrt{\pi Dt}}\frac{\varphi}{\theta}\left(1 - exp\left[-\alpha N_0\sqrt{\pi Dt}t^{1/2}\theta\right]\right) \quad (6)$$

where:

$$\varphi = 1 - \frac{exp(-At)}{\sqrt{At}}\int_0^{\sqrt{At}} exp\left(\lambda^2\right)d\lambda \quad (7)$$

$$\theta = 1 - \frac{(1 - \exp[-At])}{At} \quad (8)$$

$$\alpha = \frac{2\pi\sqrt{2MDc}}{\sqrt{\rho}} \quad (9)$$

where A is the kinetic constant for the appearance of new nucleation sites, N_0 is the initial number of nucleation sites, z is the number of exchanged electrons, F is Faraday's constant, ρ is the density of the metal as a solid, c is the metal ion bulk concentration, and D its corresponding diffusion coefficient. The function φ is directly related to the Dawson's integral and reflects the retardation of the current by slow nucleation, and θ reflects the retardation of the growth of the surface coverage as a result of slow nucleation.

The fit of the current transients of Fig. 7 using this approach (not shown here, see Fig. S.7 in the SI) gives a density of active nucleation sites No of about 1012 cm-2 and a diffusion coefficient of 6.5 × 10-6 cm2/s, which is in good agreement with previously reported values in similar systems [14,21,26,29]. The nucleation rate constant A increases with the overpotential resulting in a charge transfer coefficient of about 0.42.

We can conclude that the deposition of Rh on Ag occurs at higher overpotentials than the theoretical value and it strongly depends on the anions present in the electrolyte. In solutions containing chloride, the overpotential is lower than in sulphate media, similarly to the results obtained by Pletcher and Urbina [14,16] on GC. However, in both media the overpotential for the deposition of Rh on Ag is lower than for Rh on GC. An interesting effect observed is the appearance of an instantaneous nucleation with a 2D-growth process in a potential range between −0.1 V and −0.2 V when the electrodeposition occurs in the presence of chloride anions. Clusters with up to two monolayers of Rh can be inferred from the chronoamperometric transients in this potential region, which are corroborated by preliminary STM measurements. At higher overpotential a 2D–3D growth mechanism transition occurs. In the case of sulphate media only a 3D growth mechanism can be observed.

Table 1
Results obtained by fitting the experimental potentiostatic curves—in the potential region of peak I ($-0.170 \le E/V \le -0.120$) using Eq. (5).

Potential/V	$N_o k^2$/mol^2 cm^{-6} s^{-2}	*h*/Å	R^2
−0.12	3.28	2.26	0.997
−0.13	7.74	2.85	0.998
−0.15	29.5	3.40	0.996
−0.17	162	2.50	0.999

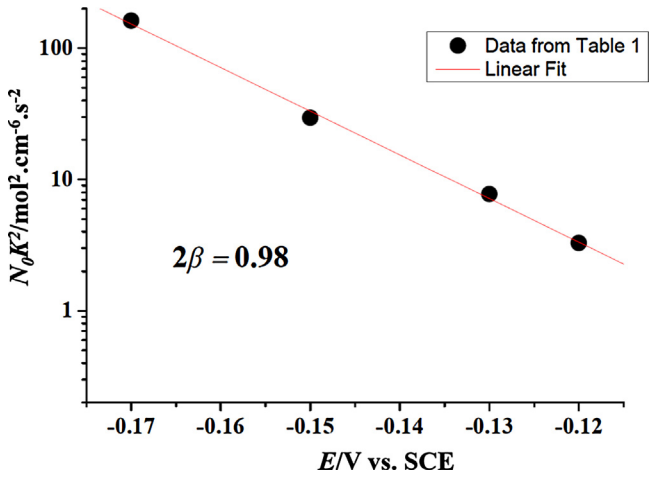

Fig. 9. Potential dependence of the product $N_o k^2$ from Table 1 obtained by fitting the current transients in the potential region of peak I with Eq. (5).

3.3. Density Functional Theory (DFT) studies of the effect of chloride on the deposition of Rh

DFT calculations were performed in order to shed some light on the experimental data. The Ag substrate was modeled as a Ag(111) surface. Computational details are given in the SI (supporting information).

The stability of Rh overlayers on Ag depends on geometric and electronic factors, as well as on the presence of stabilizing species in the environment (for example, anions that specifically adsorb in an electrochemical system). The mismatch of their lattice constants leads to lateral strains of Rh overlayers. In some cases, the chemical interaction between two different metals can be strong enough to compensate for the geometric effect, as it is the case for metallic underpotential deposition (UPD).

In a first step, the energetics of the system Rh/Ag with different amounts of Rh deposited on Ag(111) was analyzed in order to test its stability. Here, it is important to distinguish between different definitions of *energy*, which consider different references and normalizations factors.

The adsorption energy per atom, when n atoms of Rh are deposited on the Ag(111) surface at a coverage θ lower than one monolayer is defined as:

$$E_{ads.}^{Rh}(\theta) = \left[E_{nRhAgSlab}^{DFT} - nE_{RhBulk}^{DFT} - E_{AgSlab}^{DFT}\right]/n \quad (10)$$

where $E_{nRhAg_{slab}}^{DFT}$ is the resulting DFT-energy calculated when n atoms of Rh are deposited on the Ag slab. Here, the references are the n atoms of Rh in the bulk of Rh and the Ag slab, and the energy is normalized by the numbers of Rh atoms. This expression (Eq. (10)) can be interpreted as the binding energy between Rh and Ag. A positive value indicates an endothermic process for the formation of the Ag-Rh bond.

Similarly, we can define a formation energy when successive numbers L of Rh monolayers are deposited on the Ag(111) surface:

$$E_f^{Rh}(L) = \left[E^{DFT}_{LRhAgSlab} - LE^{DFT}_{RhBulk} - E^{DFT}_{AgSlab}\right]/L \quad (11)$$

This energy corresponds to the process of taking L Rh atoms from the bulk and depositing them on a 1×1 unit cell of Ag(111). Due to the periodic boundary conditions this is equivalent to the formation of L monolayers of Rh on Ag. The energy is normalized by the number of deposited layers.

A useful concept is the differential formation energy, which corresponds to the same process but taking $Rh_{L-1}/Ag(111)$ instead of Ag(111) as reference system (for $L = 1$ it gives the same energy as the total formation energy):

$$\delta E_f^{Rh} = E^{DFT}_{LRhAgSlab} - LE^{DFT}_{(L-1)RhAgSlab} - E^{DFT}_{RhBulk} \quad (12)$$

Another important definition is the surface free energy, which is given in the framework of first-principles atomistic thermodynamics by [39]:

$$\gamma(p,T) = \frac{n}{A_{cell}}\left[E^{Rh}_{Ads.} + T\Delta S\right] + \gamma^{Ag}_{Clean} \quad (13)$$

Here, the environment acts as a reservoir, such that taking or adding atoms from or to the surface does not produce neither temperature nor pressure changes. The Gibbs free energy contains an energy term (calculated by DFT), and an entropic term due to the vibrational energy of the atoms. However, because rhodium is a relatively heavy atom, the vibrational term can be neglected. The energy is normalized by the surface area A_{cell} of the unit cell. The surface energy corresponding to the clean surfaces of Ag(111) and Rh(111) is given by:

$$\gamma^{M}_{Clean}(p,T) = \frac{1}{2A_{cell}}\left[G^{M(111)}_{Slab} - n_M g_M\right] \quad (14)$$

The factor of two accounts for both equivalent surfaces of the slab (bottom and top). nM is the total number of metal atoms in the slab.

Fig. 10 shows the energetics of Rh-Ag(111) systems for different contents of Rh. On the top of the figure, energies are shown obtained according to Eqs. ((10)–(12)). In all the cases the values are positive indicating that the formations of Rh-Ag mixed systems are thermodynamically unfavorable (endothermic processes) as expected according to the chemical properties of these systems. The formation energy per atom and per layer of Rh decreases with the amount of Rh since the attractive Rh-Rh interactions are stronger than those between Rh-Ag atoms. The differential energy δE_f decreases substantially for the second Rh overlayer, approaching to zero (0.108 eV). Afterwards, it increases to a plateau that corresponds to the formation of a Rh monolayer over a Rh(111) substrate with the lateral lattice constant of Ag. We can conclude that the formation of two monolayers of rhodium is the most favorable situation in vacuum. This theoretical result supports our experimental finding (see Table 1) and the inferences from STM images [33].

From the fourth rhodium overlayer the electronic influence of the substrate atoms on the top rhodium layer is negligible; in this case geometric effects dominate over the electronic effects. At the bottom, the surface energies obtained from Eqs. ((13) and (14)) are shown. The surface energy of Rh(111) is larger than the surface energy of Ag(111) and this is in agreement with the instability of Rh overlayers on Ag. The surface energies for the clean surfaces are in agreement with both experimental and theoretical values in the literature [36,35]. When the amount of Rh on Ag(111) increases, the surface energy also increases and from the 4th layer of Rh it reaches the value corresponding to the artificial Rh(111) system calculated using the lattice constant of Ag(111). The

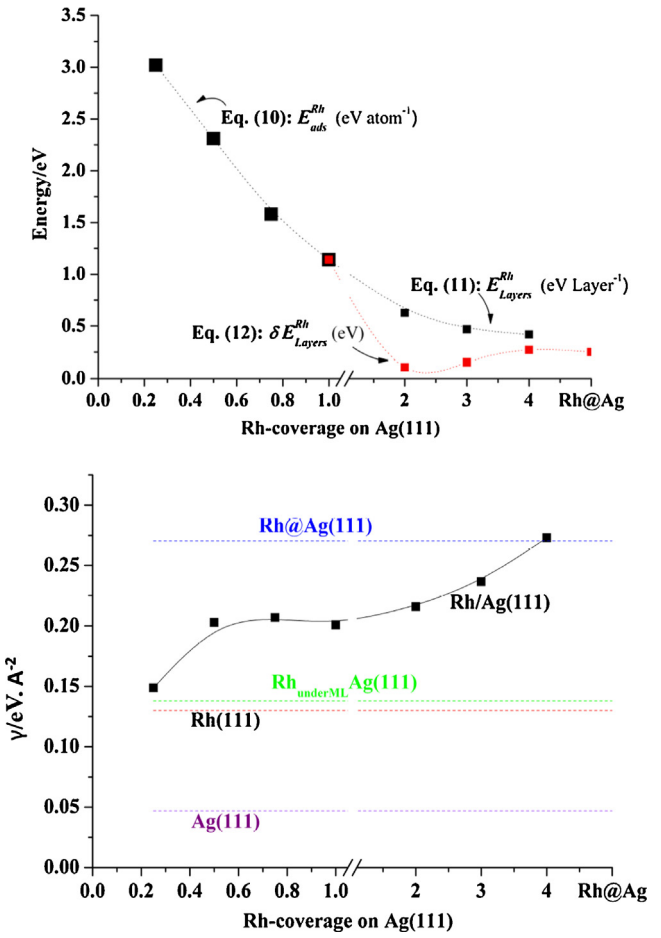

Fig. 10. Energetics of the Rh deposition on Ag(111). Top: Adsorption energy per Rh atom for a coverage lower than one monolayer as obtained from Eq. (10), formation and differential formation energy for successive monolayers of Rh as calculated from Eqs. (11) and (12), respectively. Bottom: surface energy for different amounts of Rh. The lines correspond to the clean surfaces of Ag(111) (violet dotted line) and Rh(111) (red dotted line), to the Ag(111) surface containing one monolayer of Rh intercalated below the top layer and the bulk (green dotted line) and to the surface of an artificial Rh(111) system calculated using the lattice constant of Ag(111) (blue dotted line).

formation of one monolayer underneath the surface of Ag(111) is also unfavorable ($E_f^{Rh} = 0.67eV$) and the corresponding surface energy almost similar to that of a clean Rh(111) surface.

Another fundamental question concerns the role of anions in both structural ordering of deposited metals as well as in the kinetics of metal deposition [38,37]. From our experimental results

Table 2
Energy for the co-adsorption of chlorine and Rh atoms calculated with Eq. (15) at different coverages. The adsorption energy per Cl atom on the clean Ag(111) is also shown.

E_{ads}/eV atom$_{Cl}^{-1}$	$Cl_{0.25}$	$Cl_{0.50}$	$Cl_{0.75}$	$Cl_{1.00}$
$Rh_{0.00}$	**−1.49**	**−1.17**	**-0.76**	**−0.17**
E_{ads}/eVÅ^{-2}				
$Rh_{0.25}$	0.034	**−0.026**	0.024	
$Rh_{0.50}$	0.052	0.004	**−0.043**	
			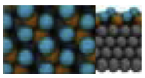	
$Rh_{0.75}$	0.058	0.006	**−0.016**	
$Rh_{1.00}$	0.055	0.009	**−0.02**	0.03

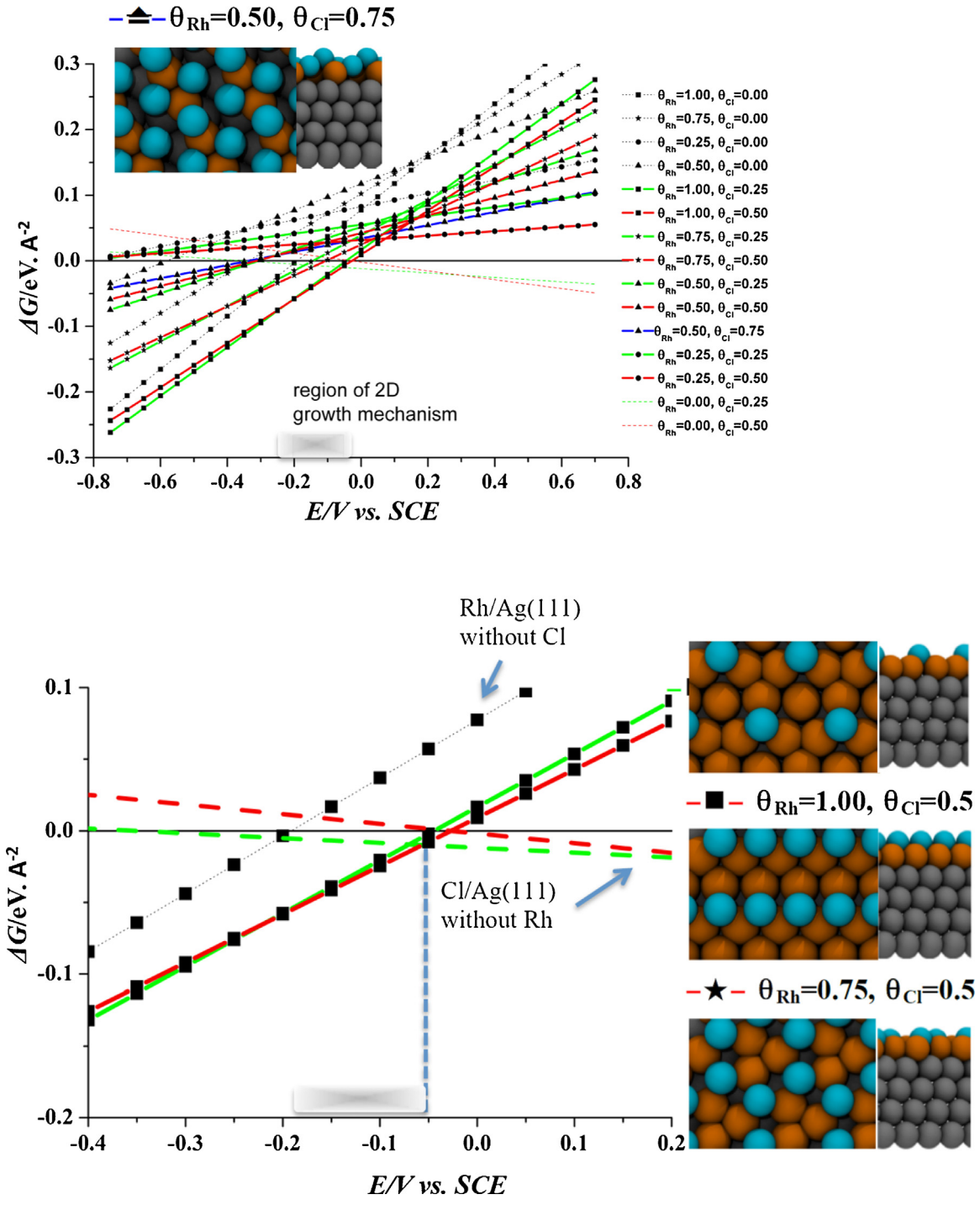

Fig. 11. Free energy for the electrodeposition of Rh on Ag(111) from the complex $RhCl_6^{3-}$ as a function of the electrochemical potential calculated by Eq. (17) according to the experimental conditions: $C_{Cl^-} = 0.5\,M$, $C_{RhCl_6^{3-}} = 5 \times 10^{-3}\,M$. Top: various representative cases at various coverage of Cl^- and Rh. The inset shows the structure of the system with the lower adsorption energy E_{ads}^{Rh-Cl} (from Eq. (15)) corresponding to the curve with triangles and blue line (see also Table 2). The shaded grey bar on the x axis shows the region where the 2D growth mechanism has been experimentally observed. Bottom: zoom of the upper plot showing the more favorable cases. The corresponding structures are shown at the side.

we expect that the presence of chloride anions greatly influences the stability of the Rh overlayers on silver electrodes. In order to investigate these effects, we have performed theoretical calculations for the co-adsorption of Rh and Cl. We have investigated different possible configurations at different coverages of both Cl and Rh atoms. In the case of bare silver we studied 48 structures and in the case of Rh-Cl we considered 111 arrangements. Here, we shall discuss only the more relevant and favourable of such structures.

It is well known from experiments that Cl binds strongly to metal surfaces and particularly to silver. This behavior has been observed in both the gas phase and the electrochemical environment. In the case of Ag(111), chloride adsorbs randomly at low coverages and at about −0.1 V vs SCE a phase transition occurs to an ordered non-

commensurate structure (aligned hexagonal 1.38×1.38, $\theta = 0.53$) [39,40]. Surface analysis techniques have revealed a remarkable similarity between the structures obtained in the gas phase and in an electrochemical environment. Experimental results of Hourani and Wieckowski [41] also indicate that chloride interact much more strongly with rhodium than with platinum.

The adsorption of chlorine on three low Miller index silver surfaces has been systematically investigated by using the first-principle density functional method with the slab model by Fu et al. [42]. Different chlorine coverages (1/6, 1/4, 1/3 and 1/2) and several adsorption geometries were considered. At low coverages ($\theta \leq 0.5$) the adsorption energy practically is constant (about -1.54 eV for the adsorption on the most favorable site (fcc) of Ag (111)). At higher coverages the repulsion between neighbors chloride induces a decrease on the adsorption strength. F. Gossenberger et al. [43] found an adsorption energy of -1.60 eV for a coverage of θ=0.11. The first row of Table 2 shows our results for the adsorption of chloride on a clean Ag(111) surface at different coverages obtained using an equation similar to the (10) but for Cl instead Rh atoms. The values are in a very good agreement with previous works.

In the case of the co-adsorption of Cl and Rh atoms, we define the adsorption energy per area of the unit cell as:

$$E_{Ads.}^{Rh-Cl}(\theta_{Rh},\theta_{Cl}) = \left[E_{nRh-mCl/AgSlab}^{DFT} - nE_{RhBulk}^{DFT} - \frac{m}{2}E_{Cl_2}^{DFT} - E_{AgSlab}^{DFT}\right]/A_{cell} \quad (15)$$

where n and m are the numbers of Rh and Cl atoms in the unit cell. Because of the possibility of the Cl adsorption on both Ag and Rh sites, $\theta_{Rh} + \theta_{Cl}$ can be higher than one.

Also the energies for the co-adsorption of Rh and Cl are shown in Table 2. The process is exothermic for some of the configurations. The most favorable case is when $\theta_{Rh} = 0.5$ and $\theta_{Cl} = 0.75$. Here the Cl atoms adsorb on combined sites between Rh and Ag, and stays at a different height of the surface (see top and side view in Table 2).

However, the above analysis is valid for the metal/vacuum interface. In an electrochemical environment the effect of the electrode potential must be included in the analysis, as was done in recent publications by Gossenberger et al. [42] based on previous work by Hansen et al. [43] has been suggested that in order to describe the adsorption of halides at electrochemical interfaces the electrochemical potential must be used as parameter.

We apply a similar procedure and calculate the free energy for the electrodeposition of Rh on Ag(111) from the complex $RhCl_6^{3-}$ in the presence of chloride anions according to our experimental conditions. We build a thermodynamic cycle (see Supporting Material) and obtain the free energy for the reaction:

$$nRhCl_6^{-3} + mCl^- + Ag_{Slab} \rightarrow nRhmCl/Ag_{Slab} + 6nCl^- + (m-3n)e^- \quad (16)$$

The corresponding dependence of the free energy on the applied potential U_{SCE} is given by:

$$\Delta G = E_{Ads.}^{Rh-Cl} + \frac{3n}{A_{cell}}\left(U_{SCE} - U_{Rh}^{0}\right) - \frac{m}{A_{cell}}\left(U_{SCE} - U_{Cl}^{0}\right) \quad (17)$$

where $U_{Rh}^{o}(= -0.190eVvsSCE$ for $C_{RhCl_6^{3-}} = 5x10^{-3}M)$ and U_{Cl}^{0}(=1.14 eV vs SCE for C_{Cl^-} = 0.5 M) are the equilibrium potentials for the redox couples $RhCl_6^{3-} + 3e^- \leftrightarrow Rh + 6Cl^-$ and $Cl_2 + 2e^- \leftrightarrow 2Cl^-$, respectively. In our case, we have to consider not only the redox couple corresponding to the chloride formation from chlorine, but also the couple for the electroreduction of Rh from the complex that we have used in the experiments.

The Eq. (17) contains the electrode potential explicitly and accounts for the electrochemical environment indirectly by using the tabulated values for the equilibrium potentials as references. Double layer capacitance effects and the varying excess charge at the metal electrode as a function of the electrode potential are not considered. This analysis is based on the thermodynamics of the systems and it does not take into account kinetic effects.

Fig. 11 shows the free energy normalized per area as obtained from Eq. (17) for the most relevant cases. In the absence of Rh, expression (17) reduces to that proposed by Gossenberger et al. describing the adsorption of chloride on Ag. Coverage of 0.50 is reached not before 0 V vs SCE in agreement with experiments [38,39].

It is noteworthy that the two last terms in Eq. (17) depending on the potential have different sign; therefore the adsorption of chloride is favored at more positive potentials, while the electrodeposition of Rh is favored at more negative potentials, as expected. Thus, not only the adsorption energy calculated by DFT but also the interplay between these two factors determines the effect of the presence of Cl in the stabilization of the electrodeposited Rh. This becomes evident in Fig. 11. In the absence of Cl, the formation of one monolayer of Rh on Ag(111) is possible only at potentials more negative than -0.2 V ($\Delta G < 0$). The presence of Cl shifts this onset by about 0.18 V to more positive potentials in agreement with the experimental finding in solution containing chloride anions. Effectively, if we compare the experiment in the presence and in the absence of chloride, in the latter case a 2D-growth mechanism has been identified at the potential range where the ΔG becomes negative in Fig. 11. Chloride coverage of about 0.25 is enough for the stabilization. Larger coverage (see the curves for $\theta_{Cl} = 0.5$ and $\theta_{Cl} = 0.75$) produces a slight increase of the free energy, probably due to repulsion between neighboring chloride. Noticeable is also that the Rh-Cl arrangement with the lowest adsorption energy ($\theta_{Rh} = 0.5$ and $\theta_{Cl} = 0.75$, blue line with triangles in Fig. 11) is not the most favorable in the potential range of interest. The ΔG becomes negative not till about -0.4 V for this configuration. This is because of the opposite effect of potential mentioned above for Rh electrodeposition and Cl adsorption given by the latter two terms of Eq. (17). The stability increases for configurations with higher coverage of Rh. These results are in agreement with the experimental evidence that chloride stabilizes the Rh first layers on silver.

4. Conclusions

We have investigated the electrodeposition of Rh on Ag electrodes using a combination of experimental and theoretical approaches. We have found that the presence of chloride stabilizes the formation of Rh clusters of monoatomic height on the surface of Ag, which evolve to bilayers. This process occurs in a potential range between -0.1 to -0.2 V vs SCE. In contrast, the electrodeposition of Rh from a sulphate rich media, follows a 3D nucleation and growth, which stresses the importance of the anions in the observed nucleation mechanism. Also, in the case of a chloride rich media, the modeling of chronoamperometric experiments has identified a clear transition from 2D to 3D growth mechanism. At more negative potentials the Rh electrodeposition takes place through a 3D growth with progressive nucleation. Although some approximations must be assumed, the theoretical ab-initio thermodynamics gives an astonishing agreement with the experiments and answers fundamental questions about the driving forces, which determine the growth mechanism. Therefore we have provided some new tools to improve the design of electrocatalysts at the nanoscale.

Acknowledgments

This work is part of the research network financed by the Deutsche ForschungsgemeinschaftFOR1376. The content has been presented and discussed in the internal meeting of this network. We thank PIP-CONICET 112-201001-00411, PICT-2012-2324 (Agencia Nacional de Promocio'n Cienti'fica y Tecnolo'gica, FONCYT, pre'stamo BID), European Union (Electrocatálisis (ELCAT)- Marie Curie fellowship, Initial Training Networks (ITN) Call: FP7-PEOPLE-2007-1-1-ITN) and DAAD. A generous grant of computing time from the Baden–Württemberg grid is gratefully acknowledged. We thank FaMAF for the funding through the Segundo Plan de Inversiones para Equipamientos 2010-2011. We thank Mohammad Al-Shakran, Ludwig A. Kibler and Timo Jacob for the private communication about preliminary characterization of our investigated system by STM. Finally, fruitfully discussions with Florian Gossenberger, Tanglaw Roman and W. Schmickler also are gratefully acknowledged.

Appendix A. Supplementary data

Supplementary data associated with this article can be found, in the online version, at http://dx.doi.org/10.1016/j.electacta.2015.08.071.

References

[1] O.A. Petrii, G.A. Tsirlina, Electrocatalytic activity prediction for hydrogen electrode reaction: intuition, art, science, Electrochimica Acta 39 (1994) 1739–1747.
[2] A.E. Alvarez, D.R. Salinas, Nucleation and growth of Zn on HOPG in the presence of gelatine as additive, Journal of Electroanalytical Chemistry 566 (2004) 393–400.
[3] M. Eldeab, T. Sotomura, T. Ohsaka, Oxygen reduction at Au nanoparticles electrodeposited on different carbon substrates, Electrochimica Acta 52 (2006) 1792–1798.
[4] L. Komsiyska, G. Staikov, Electrocrystallization of Au nanoparticles on glassy carbon from $HClO_4$ solution containing [$AuCl_4$], Electrochimica Acta. 54 (2008) 168–172.
[5] N. Toshima, H. Yan, Y. Shiraishi, Recent Progress in Bimetallic Nanoparticles: Their Preparation, Structures and Functions, Metal Nanoclusters and Catalysis in Catalysis and Materials Society: The Issue of Size Control, Elsevier, Amsterdam, 2008149–175.
[6] A.E. Alvarez, D.R. Salinas, Formation of Cu/Pd bimetallic crystals by electrochemical deposition, Electrochimica Acta 55 (2010) 3714–3720.
[7] M. Van Brussel, M.D. Amours, J. Marwan, C. Buess-herman, D. Be, Metallic and bimetallic Cu / Pt species supported on carbon surfaces by means of substituted phenyl groups, Journal of Electroanalytical Chemistry 609 (2007) 85–93.
[8] A. Groß, Tailoring the reactivity of bimetallic overlayer and surface alloy systems, Journal of Phys. Condensed Matter 25 (2009) 084205.
[9] G. Soldano, E.N. Schulz, D.R. Salinas, E. Santos, W. Schmickler, Hydrogen electrocatalysis on overlayers of rhodium over gold and palladium substrates-more active than platinum? Physical chemistry chemical physics: PCCP 13 (2011) 16437–16443.
[10] M. Smiljanić, I. Srejić, B. Grgur, Z. Rakočević, S. Štrbac, Hydrogen evolution on Au(111) catalyzed by rhodium nanoislands, Electrochemistry Communications 28 (2013) 37–39.
[11] E. Budevski, G. Staikov, W.J. Lorenz, Electrochemical Phase Formation and Growth, VCH Verlagsgesellschaft GmbH, Weinheim, 1996.
[12] P.J. Schmitz, W.-Y. Leung, G.W. Graham, P.A. Thiel, Novel metal-film configuration: Rh on Ag(100), Physical Review B 40 (1989) 11477–11487.
[13] I. Karakaya, W.T. Thompson, Bull. Alloy Phase Diagrams 74 (1986) 362.
[14] S.-L. Chang, J.-M. Wen, P.A. Thiel, S. Günther, J.A. Meyer, R.J. Behm, Initial stages of metal encapsulation during epitaxial growth studied by STM: Rh/Ag(100), Physical Review B 53 (1996) 13747–13752.
[15] L.D. Roelofs, D.A. Chipkin, C.J. Rockwell, R.J. Behm, Mechanisms of hole formation in metal-on-metal epitaxial systems: Rh/Ag(001), Surface Science 524 (2003) L89–L95.
[16] H. Li, S.C. Wu, D. Tian, Y.S. Li, J. Quinn, F. Jona, Ultrathin films of Rh on Au(001) and Rh on Ag(001): Growth mode and magnetism, Physical Review B 44 (1991) 1438–1441.
[17] L.A. Kibler, M. Kleinert, D.M. Kolb, The initial stages of rhodium deposition on Au(111), Journal of Electroanalytical Chemistry 467 (1999) 249–257.
[18] M. Arbib, B. Zhang, V. Lazarov, D. Stoychev, A. Milchev, C. Buess-Herman, Electrochemical nucleation and growth of rhodium on gold substrates, Journal of Electroanalytical Chemistry 510 (2001) 67–77.
[19] D. Pletcher, R.I. Urbina, Electrodeposition of rhodium. Part 2. Sulfate solutions, Journal of Electroanalytical Chemistry 421 (1997) 145–151.
[20] D. Pletcher, R.I. Urbina, Electrodeposition of rhodium. Part 1. Chloride solutions, Journal of Electroanalytical Chemistry 421 (1997) 137–144.
[21] E.N. Schulz, D.R. Salinas, S.G. García, Electrodeposition of rhodium onto a pre-treated glassy carbon surface, Electrochemistry Communications 12 (2010) 583–586.
[22] G. Beltramo, E. Santos, W. Schmickler, Investigation of Adsorbed Halide Layers on Single-Crystal Silver Electrodes by Second-Harmonic Generation, Langmuir 19 (2003) 4723–4727.
[23] S. Fletcher, C.S. Halliday, D. Gates, M. Westcott, T. Lwin, G. Nelson, The response of some nucleation/growth processes to triangular scans of potential, Journal of Electroanalytical Chemistry 159 (1983) 267–285.
[24] P.W. Atkins, Physical Chemistry, Sixth edition, Oxford University Press, 1998 p. 259.
[25] P. Zelenay, G. Horányi, C.K. Rhee, A. Wieckowski, Voltammetric and radioactive labeling studies of single crystal and polycrystalline rhodium electrodes in sulfate-containing electrolytes, Journal of Electroanalytical Chemistry 300 (1991) 499–519.
[26] M. Wasberg, M. Hourani, A. Wieckowski, Comparison of voltammetry of vacuum-prepared Rh (100) and Rh (111) electrodes, Journal of Electroanalytical Chemistry 278 (1990) 425–432.
[27] D.M. Anjos, M.A. Rigsby, A. Wieckowski, Underpotential deposition of copper and silver on single crystal surfaces of rhodium, Journal of Electroanalytical Chemistry 639 (2010) 8–14.
[28] E. Budevski, G. Staikov, W.J. Lorenz, Electrocrystallization Nucleation and growth phenomena, Electrochim. Acta 45 (2000) 2559–2574.
[29] J. González-García, V. Sáez, J. Iniesta, V. Montiel, A. Frías-ferrer, Electrodeposition of PbO_2 on glassy carbon electrodes: influence of ultrasound frequency, Electrochemistry Communications 4 (2002) 370–373.
[30] M. Palomar-Pardave, Detailed characterization of potentiostatic current transients with 2D-2D and 2D-3D nucleation transitions, Surface Science 399 (1998) 80–95.
[31] H.R. Thirsk, J.A. Harrison, A Guide to the Study of Electrode Kinetics, Academic Press, London, 1972.
[32] B. Scharifker, G. Hills, Theoretical and experimental studies of multiple nucleation, Electrochimica Acta 28 (1983) 879–889.
[33] Mohammad Al-Shakran, Ludwig A. Kibler, Timo Jacob. Private communication.
[34] L. Heerman, A. Tarallo, Theory of the chronoamperometric transient for electrochemical nucleation with diffusion-controlled growth, Journal of Electroanalytical Chemistry 470 (1999) 70–76.
[35] Karsten Reuter, Matthias Scheffler, Composition, structure, and stability of RuO_2(110) as a function of oxygen pressure, Physical Review B 65 (2001) 35,406.
[36] H.L. Skriver, N.M. Rosengaard, Surface energy and work function of elemental metals, Physical Review B 46 (1992) 7157–7168.
[37] D.V. Tripkovic, D. Strmcnik, D. van der Vliet, V. Stamenkovic, N.M. Markovic, The role of anions in surface electrochemistry, Faraday Discussions 140 (2008) 25–40.
[38] B.M. Jović, V.D. Jović, D.M. Drazić, Kinetics of chloride ion adsorption and the mechanism of AgCl layer formation on the (111), (100), and (110) faces of silver, Journal of Electroanalytical Chemistry 399 (1995) 197–206.
[39] Massimo Innocenti, Maria Luisa Foresti, Antonio Fernandez, Francesca Forni, Rolando Guidelli, Kinetics of Two-Dimensional Phase Transitions of Sulfide and Halide Ions on Ag(111), Journal of Physical Chemistry B 102 (1998) 9667–9676.
[40] M. Hourani, A. Wieckowski, Single crystal electrochemistry of rhodium: Anion effects and order/disorder transitions of clean and silver coated Rh (111) surfaces, Journal of Electroanalytical Chemistry and Interfacial Electrochemistry 244 (1988) 147–161.
[41] Hui Fu, Lingling Jia, Wenning Wang, Kangnian Fan, The first-principle study on chlorine-modified silver surfaces, Surface Science 584 (2005) 187–198.
[42] Florian Gossenberger, Tanglaw Roman, Axel Groß, Equilibrium coverage of halides on metal electrodes, Surface Science 631 (2015) 17–22.
[43] H.A. Hansen, I.C. Man, F. Studt, F. Abild-Pedersen, T. Bligaard, J. Rossmeisl, Electrochemical chlorine evolution at rutile oxide (110) surfaces, Physical Chemistry Chemical Physics 12 (2010) 283–290.